Progress In Electromagnetics Research, Vol. 119, 461–476, 2011

VERY MINIATURE DUAL-BAND AND DUAL-MODE BANDPASS FILTER DESIGNS ON AN INTEGRATED PASSIVE DEVICE CHIP

C.-H. Chen[1, *], C.-S. Shih[1], T.-S. Horng[1], and S.-M. Wu[2]

[1]Department of Electrical Engineering, National Sun Yat-Sen University, No. 70, Lien-Hai Road, Kaohsiung 804, Taiwan

[2]Department of Electrical Engineering, National University of Kaohsiung, No. 700, Kaohsiung University Road, Kaohsiung 811, Taiwan

Abstract—This work presents extremely compact dual-mode and dual-band bandpass filter designs based on dual-resonance composite resonators developed by using integrated passive device (IPD) technology on a glass substrate. A dual-mode bandpass filter is also devised using a symmetric composite resonator with a perturbation element of grounding inductor to determine the filter bandwidth. Additionally, a feedback capacitive coupling path on the proposed dual-mode filter is implemented to produce three transmission-zero frequencies in the stopband. Furthermore, the proposed dual-band bandpass filter is designed in a high-density wiring transformer configuration with magnetic and electric mixed coupling. In addition to individually determining the fractional bandwidth of dual passbands, the magnetic and electric mixed coupling provides multiple transmission zeros to enhance the isolation between the two passbands and greatly improve the stopband rejection.

1. INTRODUCTION

Miniature component size and multi-band operation are essential in many RF/microwave circuits. In most RF receiver fronts-ends of wireless communication systems, bandpass filters are indispensable components in suppressing the input interferences. Following the development of a dual-mode bandpass filter design method [1] based on a ring resonator configuration, considerable efforts have been

Received 1 August 2011, Accepted 17 August 2011, Scheduled 19 August 2011

* Corresponding author: Chien-Hsun Chen (D943010020@student.nsysu.edu.tw).

made to improve the construct of a square patch with a cross-slot configuration [2], a triangular open-loop resonator [3], and a square loop resonator with tree-shaped patches [4]. However, these filers require too much area since each resonator has a perimeter of one wavelength to obtain the fundamental resonance. Among the structures designed previously to reduce filter size are an octagonal meander loop resonator [5], disc-shaped open stub-loaded resonator [6], E-shaped resonator [7], and ring resonator with a saw-toothed coupling scheme [8]. Additionally, dual-band bandpass filters are implemented using the dual-mode design method. A popular solution is to impose inner stubs or loading capacitors on a dual-mode open-loop resonator [9, 10]. The inner stubs or loading capacitors developed in [9, 10] can determine the second resonant frequency and minimize the occupied area. A recent study [11] developed a single periodic stepped-impedance ring resonator configuration resulting in a controllable harmonic frequency response by designing of a number of impedance steps. In addition to dual-mode configurations, a dual-band bandpass filter can also be constructed by resonators with appropriately designed resonant frequencies. As is well known, stepped-impedance resonators (SIRs) [12, 13] can easily determine spurious frequencies by adequately selecting the impedance and length ratios in geometry. Based on SIRs structures, a dual-band bandpass filter can be readily designed using the coupling synthesis method [14]. Despite the creation of a dual-passband response by merging two sets of resonators [15, 16], a bulky circuitry space subsequently occurs. Therefore, some works have attempted to reduce the component size by developing an alternative approach to embed a defected ground structure (DGS) resonator in a dual-plane structure [17–19]. Nevertheless, the resulting designs of the microstrip bandpass filters in previous works [1–19] are still not size-competitive with low-temperature co-fired ceramic (LTCC) [20, 21] or integrated passive device (IPD) [22] bandpass filters and are difficult to integrate with RF circuits for system-in-package (SiP) applications.

This work describes a very compact dual-mode bandpass filter and a transformer-coupled dual-band bandpass filter based on glass IPD technology. Fig. 1 illustrates the cross-sectional view and material parameters of the adopted glass IPD process. IPD is characterized by the ability to produce high-Q inductors, tight wiring, and high-density capacitors using thin-film technology to minimize the component size. Furthermore, passive components adopting this technology can be easily integrated with 3D chip stacking applications. In addition to achieving a small occupied area, the proposed dual-mode bandpass filter with a feedback capacitive coupling path provides a high stopband rejection with three transmission zeros. The proposed

Material	Dielectric Constant	Loss Tangent
BCB	2.7	0.002
SiNx	7.2	0.01
Glass	5.2	0.003

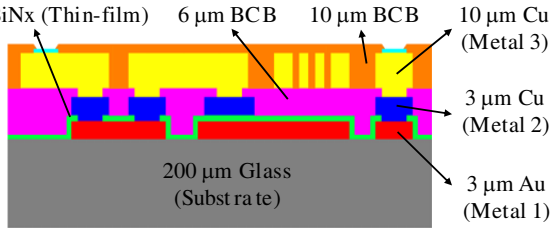

Figure 1. Cross-sectional view and material parameters of the adopted glass IPD technology.

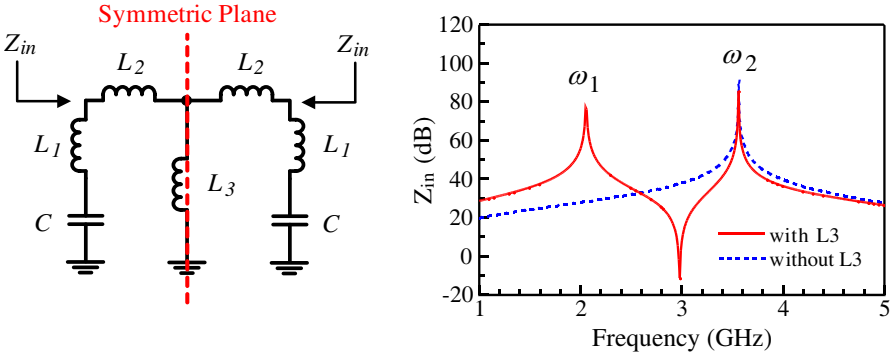

Figure 2. Proposed dual-resonance composite resonator with a grounded inductor. (a) Equivalent circuit. (b) Magnitude response of input impedance.

transformer-coupled dual-band bandpass filter with mixed coupling can independently design two passband bandwidths and realize a multiple transmission-zero creation in stopband.

2. DUAL-RESONANCE COMPOSITE RESONATORS

This work proposes two dual-resonance composite resonators for bandpass filter designs. Resonant frequencies can be obtained by analyzing the proposed equivalent circuits of the designed resonators.

2.1. Type-I Resonator with a Grounded Inductor

Figure 2(a) shows the proposed type-I dual-resonance composite resonator circuit with a grounded inductor of L_3 attached at the

symmetric plane of the circuit structure. The attached grounded inductor of L_3 provides an additional resonant frequency of ω_1 as shown in Fig. 2(b). A larger value of L_3 moves the lower resonant frequency of ω_1 away from the higher one of ω_2. For even and odd mode analysis of this symmetric circuit structure, the two angular resonant frequencies can be found as

$$\omega_1 = \omega_{even} = \frac{1}{\sqrt{(L_1 + L_2 + 2L_3)\,C}} \tag{1}$$

$$\omega_2 = \omega_{odd} = \frac{1}{\sqrt{(L_1 + L_2)\,C}}. \tag{2}$$

In the odd mode analysis, the symmetric plane in Fig. 2(a) can be viewed as a virtual ground. Therefore, L_3 has no effect on the odd mode response, and the elements of L_1, L_2, and C determine the odd mode angular resonant frequency of ω_2. In the even mode analysis, an open circuit replaces the virtual ground. The perturbation element of L_3 can be used to control the even mode angular frequency of ω_1 after designing the predetermined frequency of ω_2.

2.2. Type-II Resonator with a Parallel Capacitor

Figures 3(a) and (b) illustrate the equivalent circuit of type-II dual-resonance composite resonator with a parallel capacitor C_2 and the corresponding magnitude response of the input impedance, respectively. The parallel capacitor of C_2 separates the single-resonance into a dual-resonance response, and the two angular resonant

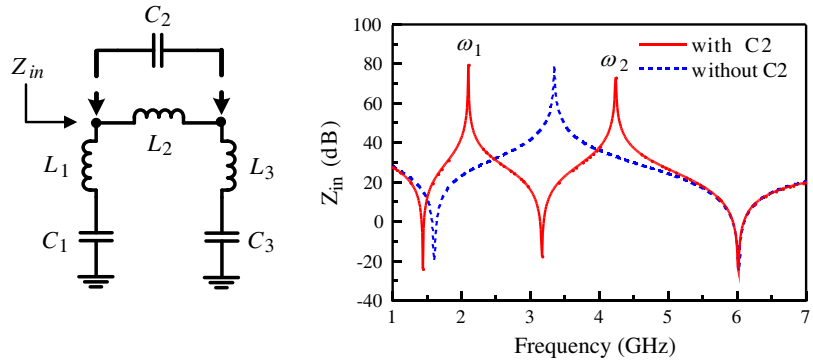

Figure 3. Proposed dual-resonance composite resonator with a parallel capacitor. (a) Equivalent circuit. (b) Magnitude response of input impedance.

frequencies can be derived as

$$\omega_1 = \sqrt{\frac{3}{4L_2C_2}} \tag{3}$$

$$\omega_2 = \sqrt{\frac{1}{4L_2C_2} + \frac{1}{L_1 + L_3}\left(\frac{1}{C_1} + \frac{1}{C_2} + \frac{1}{C_3}\right)} \tag{4}$$

The lower resonant frequency of ω_1 is determined by the L_2 and C_2, while the higher frequency of ω_2 can be determined using the other elements of L_1, L_3, C_1, and C_3.

3. DUAL-MODE BANDPASS FILTER DESIGN

3.1. Dual-mode Passband Design

The proposed type-I dual-resonance resonator with a grounded inductor can easily implement a dual-mode bandpass filter by simply placing a capacitively-coupled port (port 2) at the symmetrical tapped position with respect to port 1, as shown in Fig. 4. The source/load termination is matched using the capacitor of C_m. From knowledge of the two dominant resonant frequencies [14], the coupling coefficient k with respect to Fig. 4 can be expressed as

$$k = \frac{\omega_{odd}^2 - \omega_{even}^2}{\omega_{odd}^2 + \omega_{even}^2} = \frac{L_3}{L_1 + L_2 + L_3}. \tag{5}$$

Above equation clearly indicates that the coupling coefficient depends mainly on the perturbation element of L_3. Fig. 5 compares the dependence of the magnitude of S_{21} on three different k values of 0.4, 0.3, and 0.2, respectively. According to this figure, an increasing coupling coefficient k results in a wider bandwidth of filter. Therefore, a larger value of L_3 leads to a wider passband bandwidth for the dual-mode bandpass filter design. This same figure reveals that the center

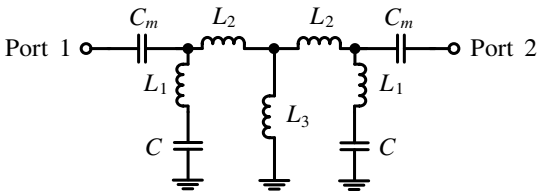

Figure 4. Equivalent circuit of the proposed dual-mode bandpass filter.

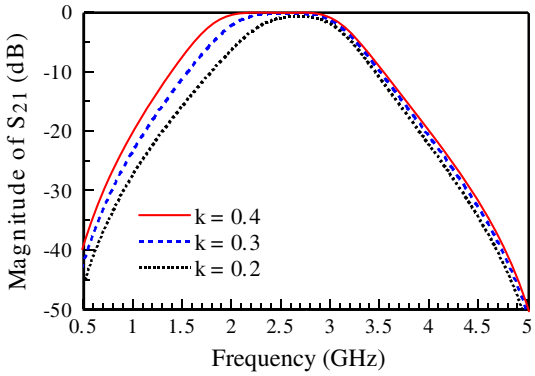

Figure 5. Comparison of operating bandwidth for the dual-mode bandpass filter design with three different coupling coefficients.

frequency of the filter decreases as the value of k increases. The relation between the coupling coefficient and center frequency can be found as

$$\omega_0 = \frac{\omega_{even} + \omega_{odd}}{2} = \frac{1}{2\sqrt{(L_1 + L_2)\,C}} \left(1 + \sqrt{\frac{1-k}{1+k}}\right). \qquad (6)$$

For the presented dual-mode bandpass filter, the inductors of L_1, L_2 and L_3 are used to obtain the desired coupling coefficient k using (5) to comply with the requirement of the fractional bandwidth design. After the k value is determined, the center frequency in (6) can be resolved by concisely designing the capacitor of C.

3.2. Transmission-zero Creation

Next consider high stopband rejection and passband selectivity for bandpass filter designs with the use of extra transmission zeros that are created by a capacitive feedback path [23]. Fig. 6 illustrates the equivalent circuit of the dual-mode bandpass filter with a feedback capacitor of C_f, where $Y_{12,filter}$ and $Y_{12,Cf}$ denote the admittance parameters of the main path and feedback path, respectively.

Figure 7(a) illustrates the magnitude and phase responses of the two paths. The three intersection points of A, B, and C label the frequencies where the two admittance parameters of $Y_{12,filter}$ and $Y_{12,Cf}$ have the same magnitude but opposite phase. The overall admittance $Y_{12,total}$ for the schematic diagram of the filter in Fig. 6 is the sum of $Y_{12,filter}$ and $Y_{12,Cf}$. As is well known, transmission zeros occur at the frequencies where the admittance parameter $Y_{12,total}$ of the two-port filters equals zero [23]. Therefore, the transmission

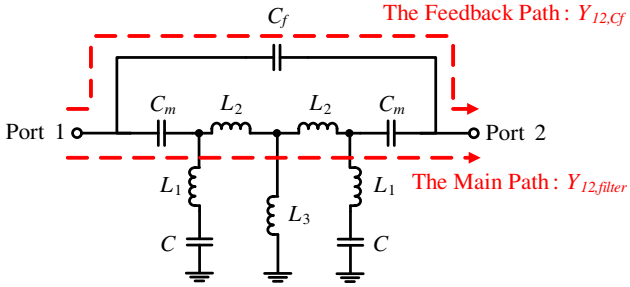

Figure 6. Equivalent circuit of dual-mode bandpass filter with a capacitive feedback path.

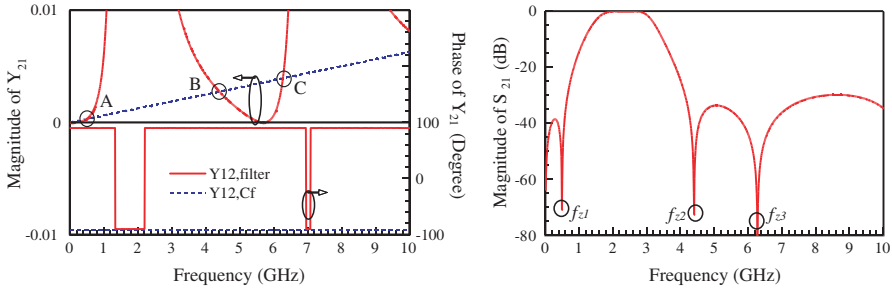

Figure 7. (a) Magnitude and phase responses of the admittance parameters of $Y_{12,filter}$ and $Y_{12,Cf}$. (b) The magnitude of S_{21} of the proposed dual-mode bandpass filter with a capacitive feedback path.

zeros occur at the frequencies of the intersection points of A, B, and C corresponding to f_{z1}, f_{z2}, and f_{z3}, respectively, in Fig. 7(b). Additionally, the locations of the three transmission zeros can be adjusted by controlling the feedback capacitor value C_f.

3.3. Experimental Results

A second-order 0.5 dB equal-ripple Chebyshev bandpass filter is designed at the center frequency of 2.45 GHz with a fractional bandwidth of 35%. The prototype element values used are $g_1 = 1.403$, $g_2 = 0.707$, and $g_3 = 1.984$. The coupling coefficient k [14] can be obtained as 0.35. To satisfy (5) and $k = 0.35$ simultaneously, the indictors of the dual-mode resonator can be selected as $L_1 = 0.8$ nH, $L_2 = 1.2$ nH, and $L_3 = 1$ nH. The capacitor is evaluated as $C = 1$ pF to meet the center frequency requirement at 2.45 GHz. The matching capacitor C_m is 1.8 pF to match the source/load impedance

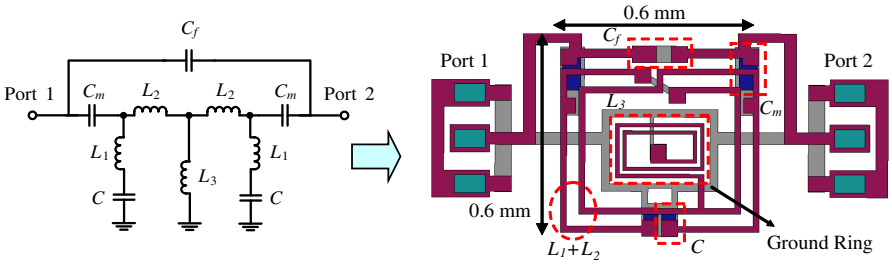

Figure 8. Proposed dual-mode bandpass filter design using glass IPD technology. (a) Equivalent circuit. (b) Corresponding layout structure.

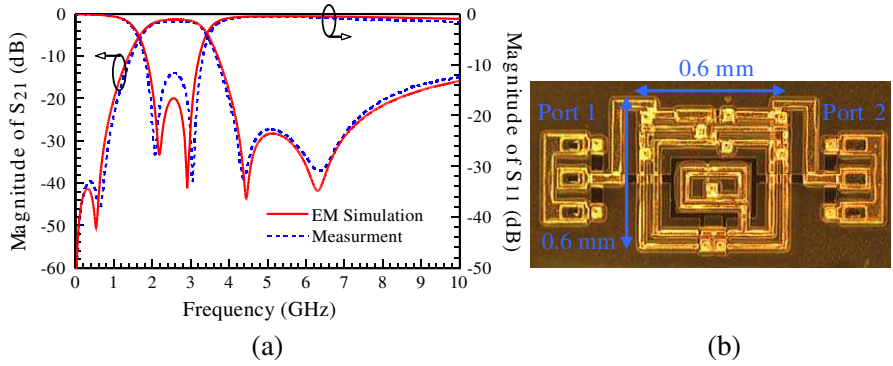

Figure 9. Results and structure of the designed IPD dual-mode bandpass filter. (a) Comparison of the magnitude of S_{21} and S_{11} between EM simulation and measurement. (b) Chip photograph.

for passband design, and the feedback capacitor is designed as $C_f = 0.08\,\text{pF}$ to create three transmission zeros in order to enhance the stopband rejection.

Figures 8(a) and 8(b) show equivalent circuit and layout structure, respectively, of the proposed dual-mode bandpass filter using IPD process on a glass substrate. The IPD technology can easily provide a high-density wiring inductor to greatly reduce the component size. The grounding ring is fabricated on metal 2 layer and used to separate the outer resonator inductors of $(L_1 + L_2)$ from the inner grounded inductor of L_3. The coil spacing and coil width of the outer inductor of L_1 and L_2 are 40 µm and 20 µm, respectively. For the inner grounded inductor of L_3, the coil spacing and coil width are 10 µm.

Figure 9(a) compares the magnitude of S_{21} and S_{11} between electromagnetic (EM) simulation and measurement for the proposed

Table 1. Comparison of measured specifications and size between the designed glass IPD dual-mode bandpass filter and those of several recent works.

Reference	Technology	Center frequency	Fractional bandwidth	Insertion loss	Component size	Using metal layers
This work	Glass IPD	2.45 GHz	35 %	1.8 dB	0.6 mm × 0.6 mm	3
[5]	PCB (Taconic CER-10)	2.3 GHz	5 %	1.4 dB	9.1 mm × 9.1 mm	2
[7]	PCB (Rogers RT5880)	2.5 GHz	2 %	1.7 dB	24 mm × 7.7 mm	2
			3.2 %	1.5 dB	25 mm × 36 mm	2
[20]	LTCC	2.45 GHz	15 %	2 dB	3.3 mm × 2.5 mm	7
[22]	Silicon IPD	2.45 GHz	15 %	1.7 dB	1.7 mm × 1.5 mm	3
			15 %	1.5 dB	1.35 mm × 1.1 mm	3

dual-mode bandpass filter design, indicating a good agreement over a frequency range of up to 10 GHz. Notably, the EM simulation is based on a full-wave analysis using ANSYS Ansoft HFSS. The measured insertion loss in the passband is less than 1.8 dB, and the passband return loss is better than 11 dB. Additionally, the feedback capacitor of C_f shown in Fig. 6 leads to three transmission zeros at 0.6, 4.4, and 6.8 GHz to suppress the outband rejection. Fig. 9(b) shows the IPD chip photograph. The occupied chip area for the dual-mode bandpass filter, excluding the feedlines and test pads, is 0.6 mm × 0.6 mm, which reveals an extremely compact size. Table 1 compares experimental results with several recent works implemented on printed circuit board (PCB), LTCC, and silicon IPD process. The comparison reveals that the proposed dual-mode bandpass filter has the smallest component size with a similar insertion loss in the passband.

4. DUAL-BAND BANDPASS FILTER DESIGN

4.1. Dual Passband Design

This work implements a transformer-coupled dual-band bandpass filter using a very compact planar transformer configuration based on the coupled resonator synthesis method [14]. Fig. 10 illustrates the equivalent circuit of the proposed transformer-coupled dual-band bandpass filter. The equivalent circuit comprises a pair of the type-II dual-resonance resonators in Fig. 3(a) with magnetic coupling k_M, electrical coupling k_E, and parasitic capacitance C_c between the two resonators. The magnetic coupling k_M results mainly from the transformer mutual inductance, and the electrical coupling k_E is

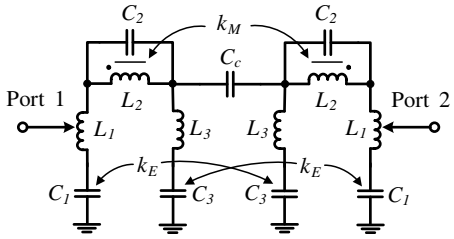

Figure 10. Equivalent circuit of the designed dual-band bandpass filter.

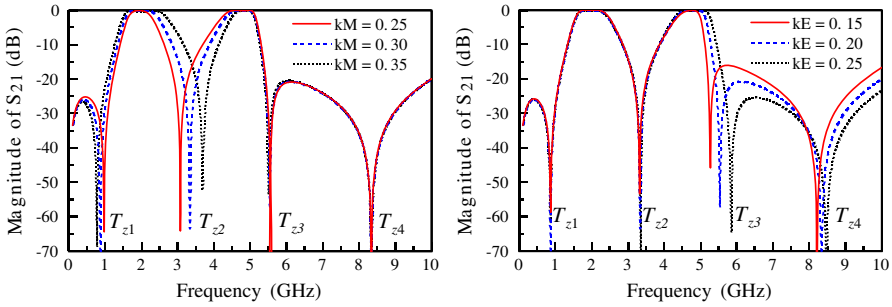

Figure 11. Comparison of the magnitude of S_{21} for the dual-band bandpass filter design with different electrical and magnetic coupling coefficients. (a) Magnitude of S_{21} with varying k_M. (b) Magnitude of S_{21} with varying k_E.

attributed to the mutual capacitance between the two capacitors of C_1 and C_3. Additionally, the source/load impedance for passband design can be matched by applying a tapped feed-line mechanism at port 1 and 2 [14] on the inductor L_1.

Figure 11 compares the simulated magnitude of S_{21} of the transformer-coupled dual-band bandpass filter by varying either the magnetic coupling coefficient k_M or the electrical coupling coefficient k_E. Fig. 11(a) shows the magnitude of S_{21} with three different k_M values of 0.23, 0.3, and 0.35 under the same k_E value of 0.2. According to this figure, the first passband bandwidth in the lower frequency range increases with an increasing k_M, which meanwhile decreases the second passband bandwidth. Fig. 11(b) demonstrates the magnitude of S_{21} with three k_E values of 0.15, 0.2, and 0.25 under the same k_M value of 0.3. One can observe from Fig. 11(b) that a larger value of k_E increases the bandwidth of the second passband without altering

the first passband response. Therefore, the bandwidth of the first passband can be designed using the magnetic coupling coefficient k_M and then the second passband is determined independently by using the electrical coupling coefficient k_E.

4.2. Transmission-zero Mechanism

In addition to achieving the desired specification of passband response, four transmission zeros of T_{z1}, T_{z2}, T_{z3}, and T_{z4} in Fig. 11 are created to increase not only the rejection at the stopband but also the isolation between the two passbands. A previous work [24] demonstrated that a design of bandpass filter with a coexistence of electric coupling and magnetic coupling can produce transmission zeros in the stopband. Based on this concept, the transmission zeros of T_{z1} and T_{z2} on both sides of the first passband come from the mixed k_M-coupling and C_c-coupling. A larger value of C_c pushes the two transmission zeros of T_{z1} and T_{z2} closer to the first passband. Similarly, the other two transmission zeros of T_{z3} and T_{z4} are derived from the combined effects of k_M and k_E. A weaker electrical coupling coefficient of k_E moves the transmission zeros of T_{z3} and T_{z4} toward the second passband. Consequently, in addition to determining the two passband bandwidths, the magnetic and electrical couplings can also create four transmission zeros to enhance the stopband rejection and the isolation between the two passbands.

4.3. Experimental Results

The proposed second-order dual-band bandpass filter is designed at the center frequencies of $f_1 = 2\,\text{GHz}$ and $f_2 = 4.8\,\text{GHz}$, and the lump element values to obtain the two desired resonant frequencies using (3) and (4) are $L_1 = 1.15\,\text{nH}$, $L_2 = 1.4\,\text{nH}$, $L_3 = 0.4\,\text{nH}$, $C_1 = 1.2\,\text{pF}$, $C_2 = 3.3\,\text{pF}$, and $C_3 = 5\,\text{pF}$. This second-order bandpass filter adopts the Chebyshev 0.5 dB equal-ripple design with the prototype elements of $g_1 = 1.403$, $g_2 = 0.707$, and $g_3 = 1.984$. The fractional bandwidths of the first and second passbands are $\Delta_1 = 30\%$ and $\Delta_2 = 20\%$, respectively. The coupling coefficients and external quality factors [14] can be estimated as $k_1 = k_M = 0.3$, $k_2 = k_E = 0.2$, $Q_{e1} = 4.7$, and $Q_{e2} = 7$.

Figures 12(a) and 12(b) show equivalent circuit and layout structure, respectively, of the designed transformer-coupled dual-band bandpass filter using glass IPD technology. The magnetic coupling coefficient k_M for the first passband is provided by designing the coil turn spacing S_{c1} of the transformer. The coupling spacing of S_{c2} between the two stubs with the capacitors of C_1 and C_3, respectively,

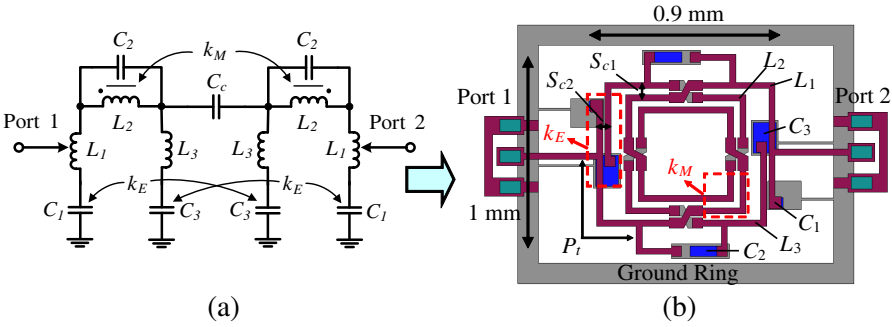

Figure 12. Proposed transformer-coupled dual-band bandpass filter design using glass IPD technology. (a) Equivalent circuit. (b) Corresponding layout structure.

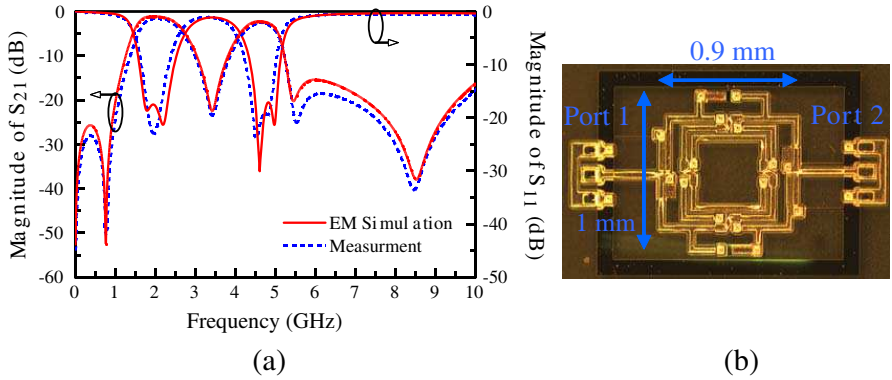

Figure 13. Results and structure of the designed IPD transformer-coupled dual-band bandpass filter. (a) Comparison of the magnitude of S_{21} and S_{11} between EM simulation and measurement. (b) Chip photograph.

supplies the electrical coupling k_E to determine the second passband response. To satisfy the calculated coupling coefficients of $k_1 = 0.3$ and $k_2 = 0.2$, the coil turn spacing of $S_{c1} = 30\,\mu\text{m}$ and the coupling spacing of $S_{c2} = 10\,\mu\text{m}$ are determined. The tapped feed position of $P_t = 0.51\,\text{mm}$ is used to match the estimated external quality factors of $Q_{e1} = 4.7$ and $Q_{e2} = 7$.

Figure 13 shows the results and structure of the glass IPD transformer-coupled dual-band bandpass filter design. Fig. 13(a) compares the magnitude of S_{21} and S_{11} between EM simulation and measurement results, showing a good agreement within 10 GHz. The

Table 2. Comparison of measured specifications and size between the designed glass IPD dual-band bandpass filter and those of several recent works.

Reference	Technology	Center frequency	Fractional bandwidth	Insertion loss	Component size
This work	Glass IPD	f_1 = 2 GHz	Δ_1 = 30 %	1.5 dB	1 mm × 0.9 mm
		f_2 = 4.8 GHz	Δ_2 = 6 %	2.5 dB	
[11]	PCB (RT/Duroid 6010)	f_1 = 2.5 GHz	Δ_1 = 5.5 %	1.9 dB	10 mm × 10 mm
		f_2 = 4.7 GHz	Δ_2 = 20 %	1.5 dB	
[16]	PCB (RT/Duroid 4003)	f_1 = 2.45 GHz	N.A.	2.5 dB	9.8 mm × 8.7 mm
		f_2 = 5.7 GHz		2.1 dB	
[21]	LTCC	f_1 = 2.4 GHz	Δ_1 = 16 %	1.7 dB	3.8 mm × 3.4 mm
		f_2 = 5.6 GHz	Δ_2 = 20 %	1.3 dB	

measured insertion losses of the first and second passbands are 1.5 dB and 2.5 dB, respectively, and the measured return losses are both better than 18 dB. The maximum attenuation between the two passbands is more than 20 dB owing to the transmission zero at 3.4 GHz. The other three transmission zeros at 0.8, 5.5, and 8.5 GHz cause a stopband attenuation of more than 20 dB. Fig. 13(b) displays the photograph of the actual device. The occupied area of the designed glass IPD dual-band bandpass filter, excluding the outer ground ring and test pads, is 1 mm × 0.9 mm. Table 2 compares the presented measurement results with those of other works using PCB and LTCC process, indicating that our work has the smallest component size with a reasonable insertion loss in the two passbands.

5. CONCLUSION

This work has developed super compact dual-mode and dual-band bandpass filter designs using the proposed dual-resonance resonators based on glass IPD technology. The proposed dual-mode bandpass filter adopts a symmetrical composite resonator with a grounded inductor. Advantages of the dual-mode filter design include an extremely small component size and ease of determining the operating bandwidth by designing the grounded inductor. Additionally, a capacitive feedback path between the input and output ports creates three transmission zeros to enhance the desired stopband rejection. Moreover, the proposed dual-band bandpass filter is implemented on a miniaturized transformer-coupled configuration. In addition, the fractional bandwidths of the two passbands are individually designed by using the magnetic and electrical coupling mechanisms.

Furthermore, the coexistence of electrical and magnetic couplings in the filter configuration introduces four transmission zeros to significantly enhance the outband rejection and improve the isolation between the two passbands.

REFERENCES

1. Wolff, I., "Microstrip bandpass filter using degenerate modes of a microstrip ring resonator," *Electronics Letters*, Vol. 8, No. 12, 302–303, 1972.
2. Zhu, L., T.-C. Boon, and J.-Q. Siang, "Miniaturized dual-mode bandpass filter using inductively loaded cross-slotted patch resonator," *IEEE Microw. Wireless Compon. Lett.*, Vol. 15, No. 1, 22–24, Jan. 2005.
3. Zhao, L.-P., X.-W. Dai, Z.-X. Chen, and C.-H. Liang, "Novel design of dual-mode dual-band bandpass filter with triangular resonator," *Progress In Electromagnetics Research*, Vol. 77, 417–424, 2007.
4. Wang, Y. X., B.-Z. Wang, and J. Wang, "A compact square loop dual-mode bandpass filter with wide stopband," *Progress In Electromagnetics Research*, Vol. 77, 67–73, 2007.
5. Esfeh, B. K., A. Ismail, R. S. A. Raja Abdullah, H. Adam, and A. R. H. Alhaeari, "Compact narrowband bandpass filter using dual-mode octagonal meandered loop resonator for WiMAX application," *Progress In Electromagnetics Research B*, Vol. 16, 277–290, 2009.
6. Deng, H.-W., Y.-J. Zhao, X.-S. Zhang, L. Zhang, and W. Zhao, "Compact dual-mode open stub-loaded resonator and BPF," *Progress In Electromagnetics Research Letters*, Vol. 14, 119–125, 2010.
7. Wei, C.-L., B.-F. Jia, Z.-J. Zhu, and M.-C. Tang, "Design of different selectivity dual-mode filters with E-shaped resonator," *Progress In Electromagnetics Research*, Vol. 116, 517–532, 2011.
8. Hsu, H.-W., C.-H. Lai, and T.-G. Ma, "A miniaturized dual-mode ring bandpass filter," *IEEE Microw. Wireless Compon. Lett.*, Vol. 20, No. 10, 542–544, Oct. 2010.
9. Wang, J.-P., L. Wang, Y.-X. Guo, Y.-X. Wang, and D.-G. Fang, "Miniaturized dual-mode bandpass filter with controllable harmonic response for dual-band applications," *Journal of Electromagnetic Waves and Applications*, Vol. 23, No. 11–12, 1525–1533, 2009.

10. Ahumada, M. D. C., J. Martel-Villagr, F. Medina, and F. Mesa, "Application of stub loaded folded stepped impedance resonators to dual band filter design," *Progress In Electromagnetics Research*, Vol. 102, 107–124, 2010.
11. Chiou, Y.-C., P.-S. Yang, J.-T. Kuo, and C.-Y. Wu, "Transmission zero design grapf for dual-mode dual-band filter with periodic stepped-impedance ring resonator," *Progress In Electromagnetics Research*, Vol. 108, 23–36, 2010.
12. Alkanhal, M. A. S., "Dual-band bandpass filters using inverted stepped-impedance resonators," *Journal of Electromagnetic Waves and Applications*, Vol. 23, No. 8–9, 1211–1220, 2009.
13. Guo, L., Z.-Y. Yu, and L. Zhang, "Design of a dual-mode dual-band filter using stepped impedance resonators," *Progress In Electromagnetics Research Letters*, Vol. 14, 147–154, 2010.
14. Hong, J.-S. and M. J. Lancaster, *Microstrip Filters for RF/Microwave Applications*, Wiley, New York, 2001.
15. Yang, R.-Y., H. Kuan, C.-Y. Hung, and C.-S. Ye, "Design of dual-band bandpass filters using a dual feeding structure and embedded uniform impedance resonators," *Progress In Electromagnetics Research*, Vol. 105, 93–102, 2010.
16. Chen, C.-Y. and C.-C. Lin, "The design and fabrication of a highly compact microstrip dual-band bandpass filter," *Progress In Electromagnetics Research*, Vol. 112, 299–307, 2011.
17. Wu, G.-L., W. Mu, X.-W. Dai, and Y.-C. Jiao, "Design of novel dual-band bandpass filter with microstrip meander-loop resonator and CSRR DGS," *Progress In Electromagnetics Research*, Vol. 78, 17–24, 2008.
18. Xiao, J.-K. and H.-F. Huang, "New dual-band bandpass filter with compact SIR structure," *Progress In Electromagnetics Research Letters*, Vol. 18, 125–134, 2010.
19. Lai, X., N. Wang, B. Wu, and C. H. Liang, "Design of dual-band filter based on OLRR and DSIR," *Journal of Electromagnetic Waves and Applications*, Vol. 24, No. 2–3, 209–218, 2010.
20. Tang, C.-W. "Harmonic-suppression LTCC filter with the step-impedance quarter-wavelength open stub," *IEEE Trans. Microw. Theory Tech.*, Vol. 52, No. 2, 617–624, Feb. 2004.
21. Joshi, H. and W.-J. Chappell, "Dual-band lumped-element bandpass filter," *IEEE Trans. Microw. Theory Tech.*, Vol. 54, No. 12, 4169–4177, Dec. 2006.
22. Frye, R. C., K. Liu, G. Badakere, and L. Yaojian, "A hybrid coupled-resonator bandpass filter topology implemented on lossy

semiconductor substrates," *IEEE MTT-S Int. Microw. Symp. Dig.*, 1757–1760, 2007.

23. Yeung, L. K. and K.-L. Wu, "A compact second-order LTCC bandpass filter with two finite transmission zeros," *IEEE Trans. Microw. Theory Tech.*, Vol. 51, No. 2, 337–341, Feb. 2003.
24. Chu, Q. X. and H. Wang, "A compact open-loop filter with mixed electric and magnetic coupling," *IEEE Trans. Microw. Theory Tech.*, Vol. 56, No. 2, 431–439, Feb. 2008.